Influence of Tertiary Gamma Prime () Size Evolution on Dwell Fatigue Crack Growth Behavior in CG RR1000

Schulz, Fiona; Li, Hangyue; Kitaguchi, Hiroto; Child, D.; Williams, S.; Bowen, Paul

DOI:
10.1007/s11661-018-4779-9

Influence of Tertiary Gamma Prime (γ') Size Evolution on Dwell Fatigue Crack Growth Behavior in CG RR1000

F. SCHULZ, H.Y. LI, H. KITAGUCHI, D. CHILD, S. WILLIAMS, and P. BOWEN

This work investigates coarsening behavior of strengthening precipitates (γ') in coarse-grained RR1000 after isothermal exposure for various times (50 to 500 hours) at 700 °C and 750 °C. The impact of these isothermal treatments is then studied by carrying out dwell (1 hour) fatigue crack growth tests at 700 °C in air. Such dwell periods can increase crack growth rates by nearly two orders of magnitude compared with baseline (0.25 Hz trapezoidal waveform) fatigue crack growth tests. Predominantly, scanning electron microscopy was used for γ' analysis. Transmission electron microscopy was also utilized when necessary. Overaging as a thermodynamically driven and diffusion-controlled process strongly affects tertiary γ' precipitates for the temperatures and treatment times investigated here. No influence of overaging on baseline fatigue behavior is observed. However, after overaging at 750 °C for 500 hours (which increases the mean tertiary γ' size by a factor of two from 17 to 37 nm), dwell crack growth rates at 700 °C are reduced by one order of magnitude. Increased dwell fatigue crack growth resistance is also measured after overaging for 100 hours at 700 °C. The potential influence of γ' distributions on dwell fatigue crack growth resistance is discussed in terms of stress relaxation behavior during dwell periods.

https://doi.org/10.1007/s11661-018-4779-9

I. INTRODUCTION

MODERN gas turbine engines are required to achieve increased efficiencies, higher performance, and maintain component life.[1] Thus, engine disk components are required to operate at increasing temperatures with higher rotational speeds, calling for optimized polycrystalline nickel-based superalloys.[2] One such alloy is a powder metallurgy (PM) alloy RR1000.[3] Coarse-grained (CG) variants of this alloy have been shown to demonstrate improved creep and dwell fatigue crack growth resistance over fine grained variants.[4,5]

The dwell fatigue crack growth behavior of such disk alloys is influenced by a number of factors such as grain size, testing temperature, R ratio, and testing environment.[3,5–12]

The evolution of strengthening precipitates (γ') under service conditions and their influence on dwell fatigue crack growth behavior is important for lifing of engine disk components.[7,13–16] Telesman *et al.*[15] reported that the size of tertiary γ' had a significant influence on dwell fatigue crack growth. The authors found that fast cooling rates after solution treatment resulted in a reduction of dwell fatigue crack growth resistance while subsequent isothermal treatments proved beneficial.[15] Li *et al.*[12] focused on dwell fatigue crack growth resistance of CG RR1000 subjected to different cooling rates after solution heat treatment and after a high-temperature stabilize treatment. It was suggested that differences of nearly two orders of magnitude in crack growth rate could result from changing tertiary γ' size and distribution alone and that the effect of overaging is most significant.[12]

This work aims to systematically study overaging behavior of coarse grain RR1000 over a range of conditions of combined temperature and time which are of potential relevance to service conditions. A number of heat treatments were applied to test pieces prior to testing to investigate the influence of overaging on dwell fatigue crack growth resistance. The study focuses on the extent to which observed dwell fatigue crack growth resistance can be explained solely by the mean sizes and distributions of tertiary γ' precipitates.

II. EXPERIMENTAL PROCEDURES

Table I shows the nominal chemical composition of the investigated material RR1000. A small block of

F. SCHULZ, H.Y. LI, H. KITAGUCHI, and P. BOWEN are with the School of Metallurgy and Materials, University of Birmingham, Birmingham, B15 2TT, UK. Contact e-mail: h.y.li.1@bham.ac.uk D. CHILD and S. WILLIAMS are with Rolls-Royce plc, Derby, DE24 8BJ, UK.

Manuscript submitted March 15, 2018.

Published online: 16 July 2018

Table I. Nominal Chemical Composition of RR1000

	Cr	Co	Mo	Al	Ti	Ta	Hf	C	B	Zr	Ni
Wt pct	15.0	18.5	5.0	3.0	3.6	2.0	0.5	0.027	0.015	0.06	52.3

material of ~ 20 × 30 × 30 mm^3 from a pancake forging was provided by Rolls-Royce plc. It had experienced a super-solvus treatment at 1170 °C for 2 hours to produce a coarse-grained variant, followed by a standard post-solution aging treatment of 16 hours at 760 °C. The as-received block was then divided into eight ~ 10 × 10 × 10 mm^3 cubes and subsequently given different treatments. Two samples were kept in the as-received condition, and isothermal overaging treatments were applied to the other six samples at various temperatures (700 °C and 750 °C) and time periods (50, 100, and 500 hours) under zero stress. All γ' distributions presented in this current paper are derived from these heat-treated samples alone.

For γ' distribution analyses, each sample was etched electro-chemically in a 10 pct orthophosphoric acid solution with de-ionized water at 2.5 V for 1 to 2 seconds (to remove the γ matrix), following conventional metallographic specimen polishing. This very short etching time removed only a thin layer of γ matrix and revealed mainly the γ' particles intercepting the polished surface. Some small tertiary γ' particles not intercepting polished surface but within the thin eroded surface layer can also been revealed. To observe the potential splitting behavior of secondary γ' precipitates, a further etching technique which removes γ' precipitates was employed. For this analysis of secondary γ' precipitate shapes alone, a two-part chemical etching method (Part I: 15 mL·H_2O, 150 mL·HCl, 2.5 g MoO_3; Part II: 15 mL·HNO_3, 25 mL·H_2O and 30 mL part I[17]) was applied to some samples.

A field-emission JEOL 7000F scanning electron microscope (SEM) was used to observe γ' distributions. Images were taken with a fixed acceleration voltage of 20 kV. Different magnifications were applied for tertiary γ' analysis (100,000×) and secondary γ' analysis (25,000×). In order to observe any changes in population of the γ' precipitates, five images were taken under secondary electron mode. ImageJ software was used to analyze the respective γ' size distributions. Prior to isothermal treatments at 700 °C and 750 °C, the as-received microstructures were analyzed to provide a baseline reference.

In addition to SEM analysis, the size of tertiary γ' particles was also characterized using a FEI TECNAI F20 transmission electron microscope (TEM) in scanning mode (STEM) with a dark-field detector. This is particularly important for the as-received samples, and for samples exposed at 700 °C, as there are significant amounts of small particles less than 5 nm that cannot be adequately resolved by the SEM. After conventional metallographic specimen preparation, the material was etched electro-chemically as described above, but for 5 to 7 seconds. Following this deeper etching, both mounting material and approximately 1 mm of sample material were blanked off prior to carbon coating to a thickness of 60 to 70 nm. Subsequently, the coated surface was scored to produce areas with a diameter of 3 mm. The sample underneath the carbon coating was then electro-chemically polished using 20 pct perchloric acid in methanol with 3 V for approximately 60 seconds, followed by an increase in voltage (~10 V) for 5 seconds, after which, the sample was slipped into de-ionized water at an acute angle. The floating C squares were collected onto Cu electron microscope grids for TEM analysis.

In order to investigate the influence of different tertiary γ' distributions on dwell fatigue crack growth resistance, five as-received specimens were subjected to different isothermal overaging treatments. The as-received material had received the same standard post-forging heat treatment as described above. Prior to overaging heat treatments, each specimen was encapsulated in glass tubes with Ar backfill in order to minimize oxidation. After each heat treatment, the glass capsule was broken and the specimen was allowed to cool in air.

The dwell fatigue crack growth tests were carried out on corner notched test specimens with a 7 × 7 mm^2 cross section. They are all extracted from a different pancake forging. In order to minimize any grain size variations, all test specimens were extracted from the same position in the radial direction and in a closely packed row. The average grain size and standard deviation for this row of test pieces were 28 μm and ± 18 μm. Tests were performed at 700 °C in air. After pre-cracking, a 0.25 Hz trapezoidal (1-1-1-1 s) loading waveform was applied. A 1-hour dwell segment at peak load (1-3600-1-1 s) was then introduced at a ΔK value of ~ 25 MPa$\sqrt{m}$. A direct current potential drop (DCPD) technique was used to measure the crack length during testing. Crack lengths were validated from beach marks on the fracture surface with reference to the measured PD values and standard calibration functions. Note that an initial ΔK value of ~ 25 MPa$\sqrt{m}$ was chosen deliberately to avoid potential crack growth retardations which can often be observed at lower ΔK values.[12]

Fractography was performed by first inspecting using a Nikon optical microscope equipped with a GXCAM camera, followed by more detailed observations using a Philips XL-30 SEM.

Stress relaxation tests were carried out on as-received and overaged (500 hours at 700 °C) samples using a round bar test piece geometry with a diameter of 5.7 mm and a gauge length of 30 mm. The test pieces were extracted in close proximity to the corner notched specimens from the same pancake forging. A high-temperature extensometer was used to enable the

tests to be conducted under strain control. A strain of 1 pct was applied in 3 seconds and then maintained over a period of 50 hours. Both load and strain were recorded during the entire duration of the test using LabView software.

III. RESULTS AND DISCUSSION

A. *Isothermal Overaging Treatments*

SEM results for the mean size and standard deviation of secondary γ' and tertiary γ' precipitates for all

Table II. γ' Precipitate Mean Diameter with the Respective Standard Deviation for All Thermal Treatment Conditions (The Respective Total Number of Samples Involved in the Individual Analysis is Given in Brackets)

		Exposure Time (h)			
	Exposure Temperature (°C)	As-received	50	100	500
Secondary γ' (nm)	700	174 ± 46 (1489)	177 ± 48 (1494)	182 ± 47 (1292)	199 ± 57 (1127)
	750	176 ± 50 (1320)	205 ± 64 (986)	189 ± 56 (1283)	203 ± 59 (1137)
Tertiary γ' (nm)	700	16 ± 3.9 (427)	18 ± 4.5 (440)	20 ± 4.9 (431)	25 ± 5.9 (295)
	750	17 ± 4.0 (419)	28 ± 6.6 (347)	31 ± 7.2 (258)	37 ± 7.7 (109)

The average grain size of the isothermal treatment samples is 34 μm with a standard deviation of 25 μm.

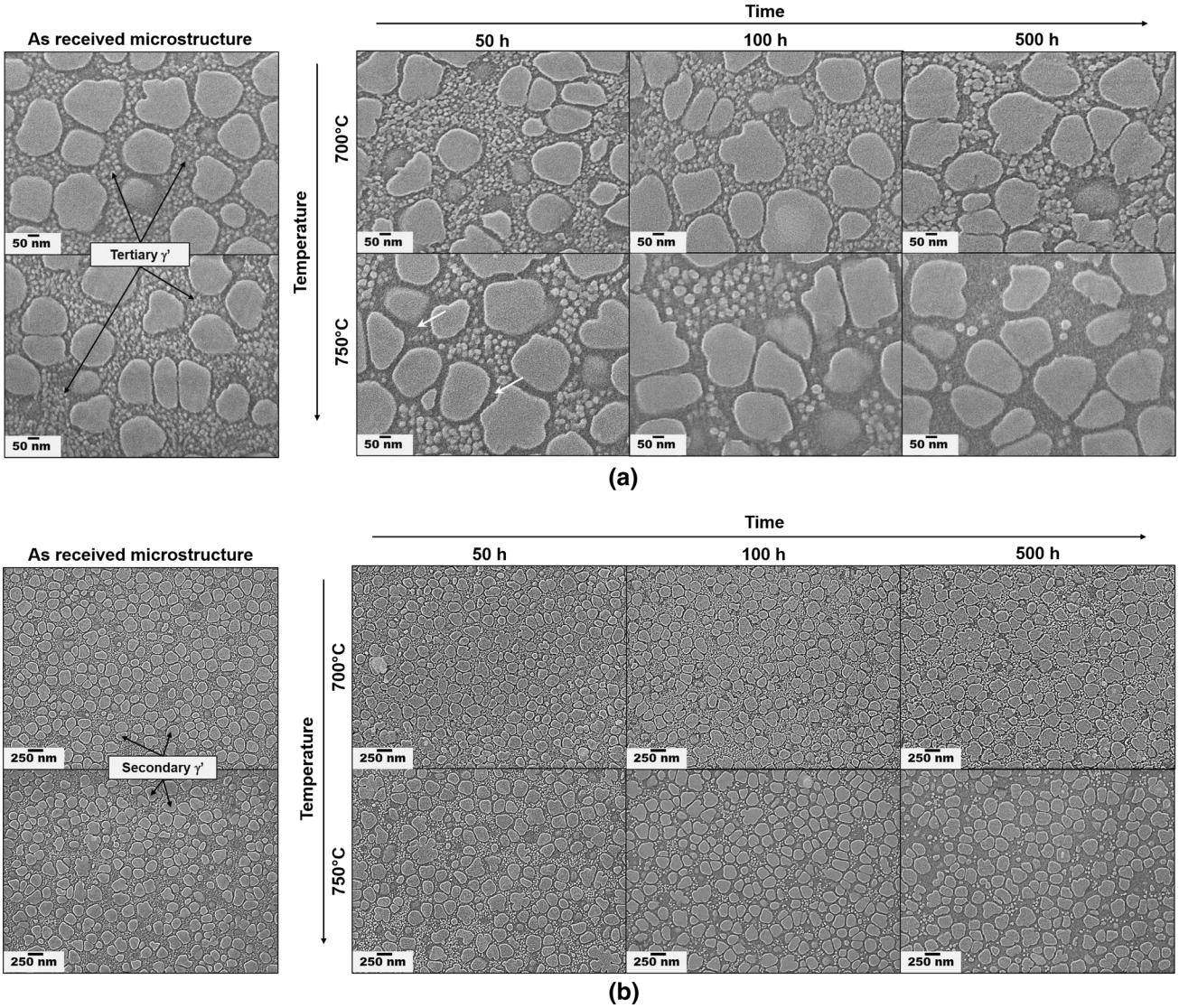

Fig. 1—Representative SEM micrographs showing the evolution of tertiary γ', (*a*), and secondary γ', (*b*), after various thermal exposure times at 700 °C and 750 °C. Note that the white arrows in the micrograph of 50 h exposure at 750 °C in (a) indicate areas where tertiary γ' precipitates are likely to have dissolved.

conditions are given in Table II. In terms of measurements given in Table II, all observations of the increase of mean values of tertiary γ' on thermal exposure can be shown to be statistically significant (against a standardized "*t*" test, for two sample populations assuming unequal variances), even for exposure at 700 °C for 50 hours. The is due to the large number of observations, but it is difficult to attach too much physical significance to an increase of mean size from 16 to 18 nm as shown in Table II. The volume fraction of γ' in equilibrium for both thermal exposure temperatures (700 °C and 750 °C) and the prior standard aging temperature (760 °C) is estimated by thermodynamic calculations (using Thermo-Calc. software with the TTNi8 database) to be 45 to 46 pct. The evaluation of volume fractions presents significant challenges experimentally, particularly related to the electrochemical etching procedure which can introduce sources of uncertainty when determining the γ' volume fraction. In the current work, γ channels can often be densely packed with tertiary γ' precipitates and attention is directed particularly towards careful measurement of the mean sizes of γ' precipitates (both secondary and tertiary), Table II. However, at the higher thermal exposure temperature of 750 °C, it can be seen from micrographs alone (Figure 1) that the volume fraction of tertiary γ' (in γ channels) reduces significantly between exposure time of 50, 100, and 500 hours.

Firstly, the as-received CG RR1000 material was analyzed with respect to both secondary and tertiary γ' size distributions. Two samples have been analyzed here which closely represent the starting microstructures for the overaged samples at 700 °C and 750 °C respectively. The differences seen between the two samples are very small, as shown in Table II, as all samples in this part of the study were from a small block of material extracted from a large pancake forging. This allows any subtle changes to be measured and compared, which is essential for the current study. The mean diameter and standard deviation for secondary γ' and tertiary γ' precipitates are 174 ± 46 and 16 ± 3.9, and 176 ± 50 and 17 ± 4.0 nm from the two as-received samples.

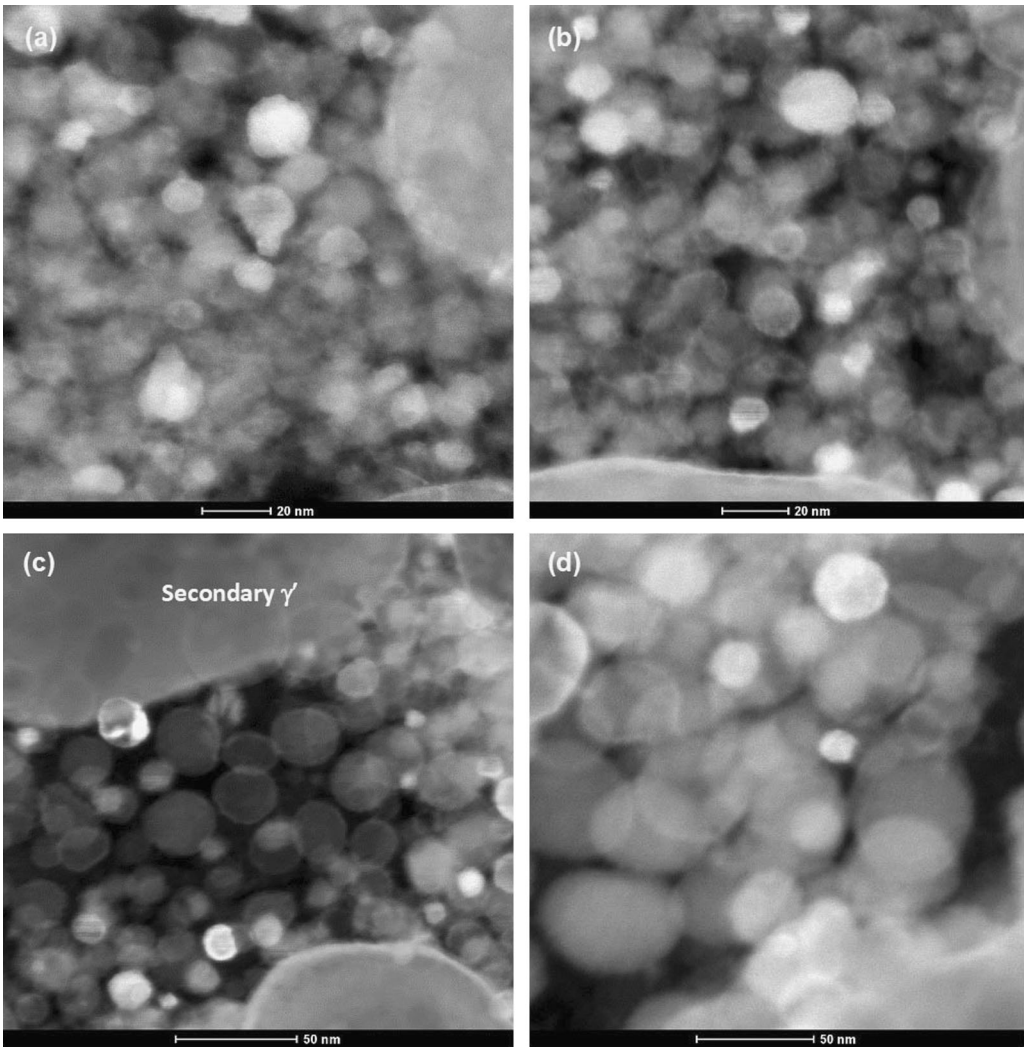

Fig. 2—Representative STEM dark-field micrographs showing tertiary γ' precipitates after different thermal exposure time at 700 °C: (*a*) as-received, (*b*) 50 h, (*c*) 100 h, and (*d*) 500 h. Note the different magnifications between (a) and (b) and (c) and (d).

Table III. Comparison of SEM and STEM Results of Tertiary γ' Precipitate Mean Diameter with the Respective Standard Deviation for the Thermal Treatments at 700 °C

	Exposure Time (h)			
Method	As-received	50	100	500
SEM	16 ± 3.9 (427)	18 ± 4.5 (440)	20 ± 4.9 (431)	25 ± 5.9 (295)
STEM	11 ± 3.2 (546)	11 ± 2.9 (420)	14 ± 4.6 (824)	21 ± 10.6 (408)

SEM micrographs of tertiary γ' precipitates from exposed material are shown in Figure 1(a) and compared with those for the original, as-received condition. Tertiary γ' size distributions of the samples heat treated at 700 °C were also investigated under STEM. Representative micrographs are shown in Figure 2. A comparison between SEM and STEM results is provided in Table III. Table III shows the results from STEM are consistently smaller than those from SEM. This can be attributed in part to the improved resolution of STEM, enabling smaller particles to be detected and measured. It could also be a consequence of the SEM detecting a high number of secondary electrons along the edge of γ' particles, which could lead to the precise face of the precipitates being obscured in the conversion to a binary image. However, using SEM, it is possible to analyze particles over a much larger area, and the trends in particle size shown by the two techniques are the same. In Figure 2, the trend can be clearly seen for a thermal exposure temperature of 700 °C. There is very little change in particle size after 50 hours (compare Figures 2(a) and (b)), some coarsening can be observed after 100 hours, and significant coarsening after 500 hours. This is consistent with SEM images in Figure 1(a) and Tables II and III. Hence, the results from the SEM method will be considered in later discussion.

By plotting average tertiary γ' size against exposure time (Figure 3), also from Table II and Figures 1, 2, it is clear that tertiary γ' can coarsen when exposed to temperatures of 700 °C and 750 °C. Coarsening occurs more rapidly at 750 °C. It is apparent at this temperature that coarsening is accompanied by a reduction in the volume fraction of tertiary γ' particles with channel areas often becoming free of tertiary γ' precipitates (Figure 1). Of note, the remaining tertiary γ' precipitates are located towards the middle of such channels away from secondary γ' precipitates. Note that this trend is supported by a reduction in the total number of tertiary γ' precipitates observed in SEM characterization from 419 in the as-received condition to 109 in the 500 hours aged condition (Table II) and counted within a fixed area (five randomly selected images at ×100,000 magnification). Relatively smaller differences in tertiary γ' size and distributions were found between the samples that received isothermal exposure at 700 °C. However, even these differences in tertiary γ' mean size are suggested to be statistically significant by t test results. At 700 °C, a noticeable change in tertiary γ' mean size is observed after 100 hours and a reduced number of tertiary γ' precipitates were observed after 500 hours. Closer analysis shows that isothermal treatment results

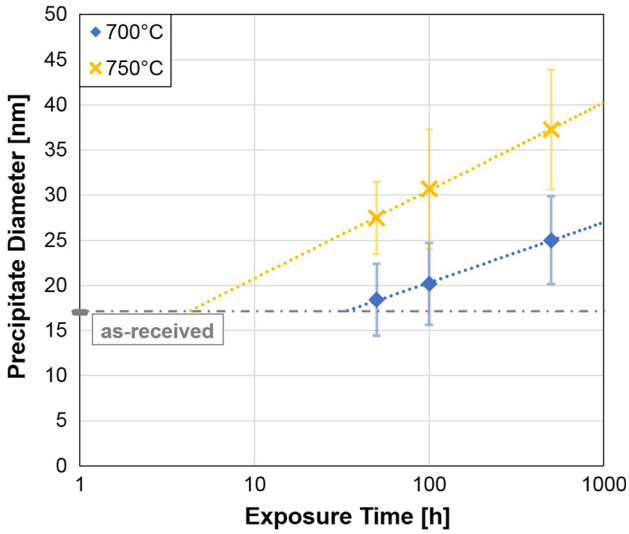

Fig. 3—Tertiary γ' coarsening behavior in RR1000 after various thermal exposure conditions obtained from SEM analysis. Note that the error bars indicate ± one standard deviation.

in a total increase in tertiary γ' size after 500 hours from 17 to 25 nm at 700 °C and from 17 to 37 nm at 750 °C (see Table II). The histograms of tertiary γ' after various overaging conditions are shown in Figure 4 in terms of precipitate diameter.

To complete the microstructural analysis, secondary γ' precipitates were also analyzed. The associated micrographs from all isothermal treatment conditions are shown in Figure 1(b), and the results are summarized in Table II and Figure 5. Coarsening now shows a less obvious trend: while isothermal overaging treatment at 700 °C results in a continuous coarsening behavior with time, such treatment at 750 °C for 50 and 500 hours both result in a larger equivalent diameter (205 and 203 nm, respectively) than that for the intermediate duration of 100 hours (189 nm). Similar results were recently reported by Chen *et al.*[18] in which RR1000 was subjected to isothermal overaging treatments at 800 °C for up to 8 hours in 0.5 hours of intervals. Size evolution of secondary γ' seemed to cycle between splitting to a spherical morphology and coarsening to a "flower-like" morphology. The results of this study are consistent with this phenomenon of cyclic evolution, as suggested by the images in Figure 6. After applying a MoO_3 etchant, more spherical secondary γ' and fewer flower-like γ' precipitates are present after 100 hours at 750 °C than for both other treatment durations of 50 and 500 hours. In the current study, the

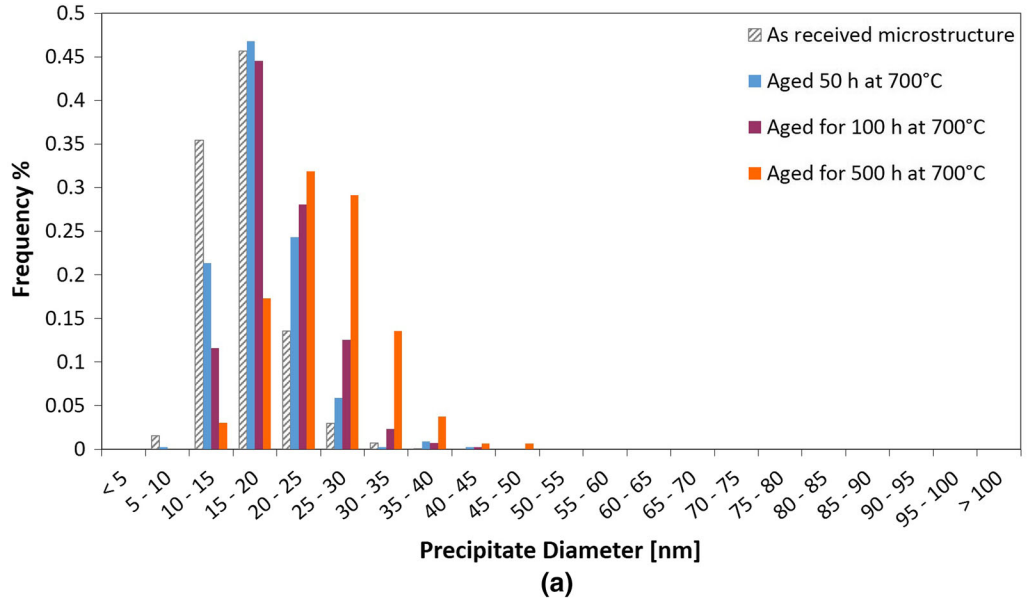

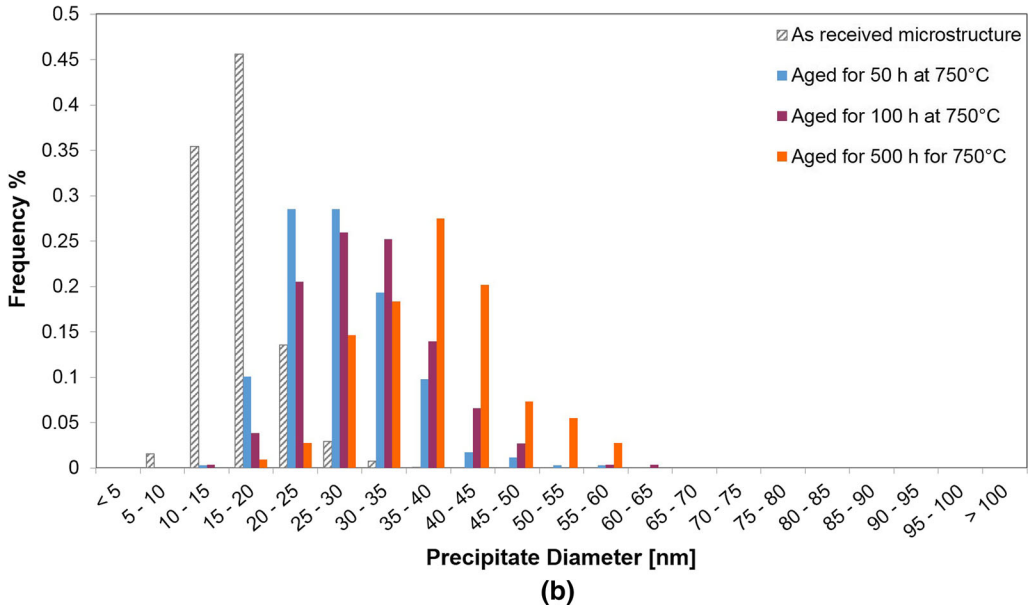

Fig. 4—Tertiary γ' distribution histograms for overaging at (*a*) 700 °C and (*b*) 750 °C based on SEM analysis.

cycles appear to occur with longer intervals compared to the results reported by Chen *et al.*[18] and which can be attributed plausibly to the lower temperature of 750 °C.

Assuming γ' evolution follows the principle of diffusion-controlled particle coarsening, based on the Lifshitz and Slyozov, and Wagner (LSW) theory, coarsening can be described by[19–21]

$$\langle r^3 \rangle - \langle r_0^3 \rangle = kt \qquad [1]$$

with r as the average particle radius after an elapsed time t of an isothermal treatment, r_0 as the average onset particle radius for coarsening, and k as a rate constant. The heat treatment time against the r^3 of secondary and tertiary γ' for the investigated conditions can be seen in Figure 7. The evolution of secondary and tertiary γ' after isothermal exposures of up to 500 hours at 700 °C (crosses and open triangles, respectively) follow Eq. [1] with rate constants of 640 and 2.8 nm^3/h, respectively. With a treatment duration of up to 500 hours at 700 °C, the current results for tertiary γ' broadly agree with findings by Zhao *et al.*[22] using a new generation Ni superalloy exposed to 704 °C for various durations (illustrated by the broken line with a rate constant of 3.2 nm^3/h). In the previous study, samples were water quenched after super-solvus heat treatment which produced a unimodal γ' distribution in the subsequent isothermal treatment.[22]

It can clearly be seen that the coarsening behavior of tertiary γ' at the 750 °C treatments did not follow Eq. [1]. The initial coarsening is rapid up to 100 hours. Between 100 and 500 hours, there appears to be a reduction in coarsening rate. SEM micrographs of these

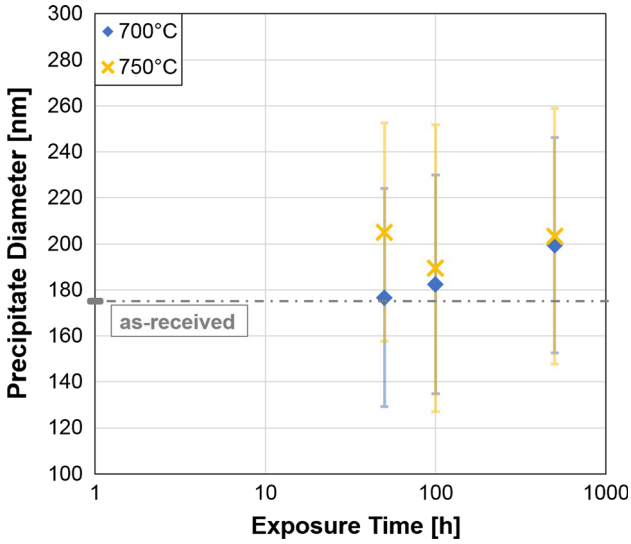

Fig. 5—Secondary γ' coarsening behavior in RR1000 when exposing the as-received material to elevated temperatures for prolonged amounts of time based on SEM analysis with the respective ± one standard deviation indicated by the error bars.

conditions show a clear reduction in the volume fraction of tertiary γ' between 100 and 500 hours. After 500 hours, there are very few tertiary γ' particles remaining. This suggests that application of Eq. [1] for this condition maybe inappropriate. Applying Eq. [1] separately to secondary and tertiary γ' could lead to misinterpretation as these two types of precipitates are not independent as the coarsening of secondary γ' will be at the expense of disappearing tertiary γ'. The fact that it was possible to apply Eq. [1] at 700 °C suggests that this effect is less pronounced at this lower temperature. However, care must be taken to interpret the coarsening rate constant, k, as it depends largely on the initial average particle size. At 700 °C, the k constant of secondary γ' is ~ 220 times larger than that of tertiary γ'. This does not imply that the coarsening rate of secondary γ' was 220 times faster than that of tertiary γ'. The k values can only be used to directly compare coarsening rates if the initial particle size and distribution are the same.

IV. DWELL FATIGUE CRACK GROWTH RESISTANCE

It is understood that the dwell fatigue crack growth resistance of CG RR1000 at 700 °C is sensitive to tertiary γ' size and distribution. Tertiary γ' size and distribution depend both on cooling rates after supersolvus solution heat treatments, and on subsequent aging heat treatments. The influence of different cooling rates followed by a standard aging heat treatment, and high-temperature stabilize aging heat treatment (HTS) on dwell fatigue crack growth resistance in CG RR1000 has been investigated previously.[12] Using a testing procedure that sequentially alternates loading blocks of fast cycling (1-1-1-1) and one-hour dwell cycling

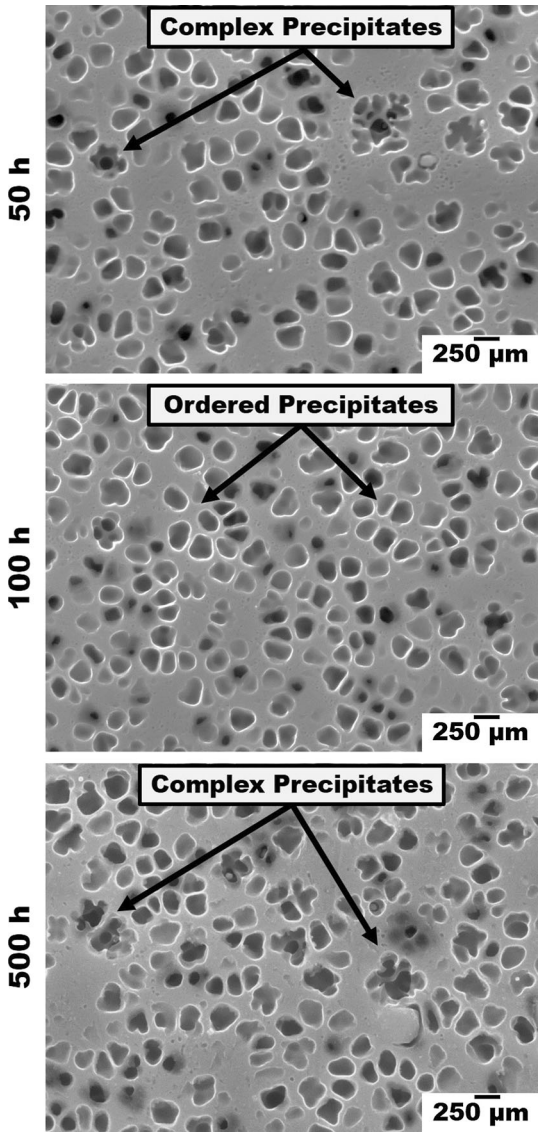

Fig. 6—Secondary γ' after isothermal treatment at 750 °C displaying different precipitate shape characteristics revealed by MoO_3 etchant.

(1-3600-1-1), increased crack growth resistance was observed for slower cooled (SC) and HTS conditions compared to a faster cooled (FC) condition. The SC and HTS test pieces both demonstrated crack growth retardations at lower mechanical driving forces, $\Delta K <$ 24 MPa$\sqrt{m}$, and decreased "continuous" crack growth rates at higher mechanical driving forces, $\Delta K >$ 29 MPa$\sqrt{m}$, compared to those from FC test pieces which showed faster crack growth rates for the whole ΔK range tested (20 to 40 MPa$\sqrt{m}$), see Figure 8(a).

Besides the unusual crack growth retardation behavior shown in SC and HTC test pieces, an interesting phenomenon was further observed when starting dwell block cycling at a higher ΔK value of 30 MPa$\sqrt{m}$ on test pieces possessing the same microstructure as in the SC sample. Without the first period of dwell block loading, the crack growth rate data are noticeably higher, Figure 8(b) compares the dwell fatigue crack growth data of these two tests (note that SC in Figure 8(a) was

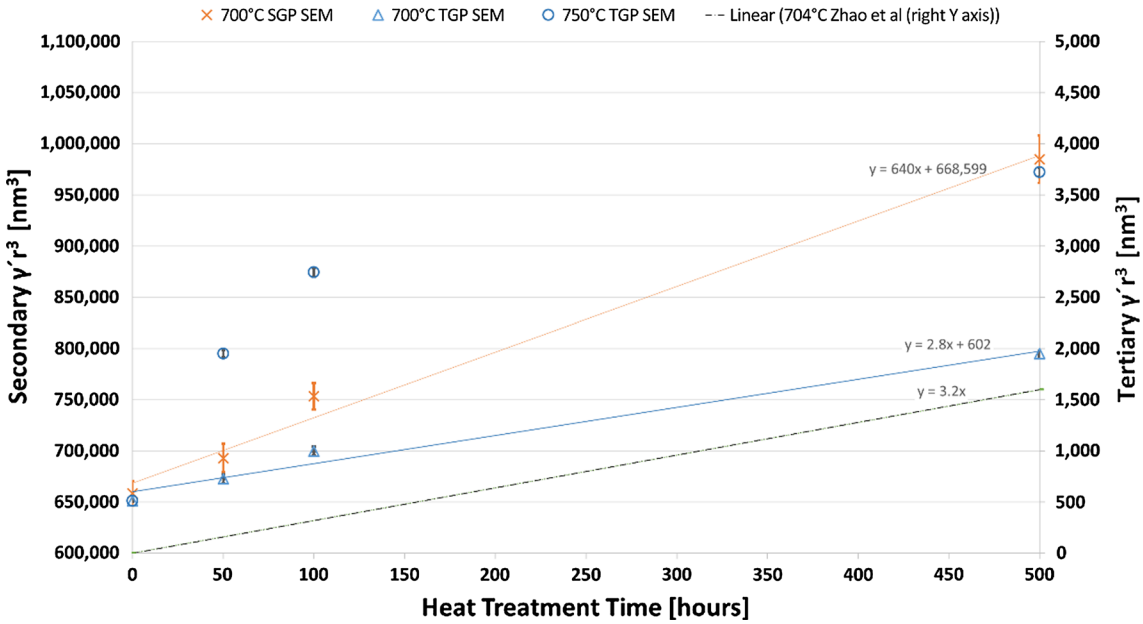

Fig. 7—Relationships of r^3 *vs* isothermal treatment time of the current study with comparisons to other work.[21] Note that *Y* axis for secondary γ' (SGP) is on the left and tertiary γ' (TGP) on the right, respectively.

replotted as SC_1 in Figure 8(b)). It was only realized after examining the microstructure of the SC sample after testing that the test piece underwent overaging while it was tested. Figure 8(c) shows the microstructure after testing which clearly shows signs of overaging as we have discussed earlier. Hence, it is logical to suggest that the crack growth curve obtained for the second dwell period of the SC condition was affected by overaging that had occurred during the first dwell period. Note that it took ~ 238 hours for the SC/SC_1 test piece to reach the second block of dwell loading. The second dwell period lasted another 138 cycles (~ 138 hours). Whereas for SC_2 the total number of dwell cycles is 43 (~ 43 hours), which is much fewer than that of the second dwell period of SC/SC_1.

These experiments reveal some important characteristics of dwell fatigue crack growth resistance: dwell crack growth resistance is sensitive not only to the starting microstructure, but also to the loading history owing to its time-dependent nature. Additionally, it can be inferred from Figure 8 that the effect of overaging could be more significant than that of cooling rate (compare for example the difference between SC_1 and SC_2 to the difference between FC and SC_2). A major study is ongoing to address such intricate interactions between various factors, and here, the current study is focused primarily on the influence of overaging.

Clearly, using a higher initial ΔK (25 to 30 MPa$\sqrt{m}$) can limit on-test overaging and allow the effects of overaging to be studied systematically. It is also convenient to compare crack growth rates in a regime of near continuous crack growth rate increases with ΔK increases, and thus to identify the minimum overaging condition required to improve dwell fatigue crack growth resistance. The results of dwell crack growth resistance curves for various overaging conditions (da/dN *vs* ΔK) under 1-3600-1-1 dwell fatigue loading are shown in Figure 9, together with their baseline fatigue crack growth data obtained under 1-1-1-1 fatigue cycling. The trend lines of associated data published previously[12] are also shown for comparison. The results can be divided into three groups: (i) a 50-hour treatment at 700 °C shows the same crack growth resistance to those from the non-exposed test pieces (both have shown crack growth rates of close to two orders magnitude higher than those of baseline fatigue crack growth); (ii) the severely overaged condition of 500 hours at 750 °C, produces the lowest dwell crack growth rates of all overaging conditions with a reduction of one order of magnitude in dwell crack growth rates from those of the as-received condition, and one order of magnitude faster than those rates observed during baseline fatigue crack growth; and, (iii) all other isothermal treatment conditions which demonstrate intermediate dwell crack growth resistance (exposure conditions of 100 hours at 700 °C, 500 hours at 700 °C, and 50 hours at 750 °C). The condition of 100 hours aging at 750 °C was not tested due to a limitation of material, however, it is predicted to show improved dwell fatigue crack growth resistance. It is noteworthy that continuous cycling during baseline fatigue is not affected by such microstructural changes and crack growth is controlled by a different mechanism. A fully transgranular fracture surface morphology is observed for baseline fatigue, instead of a fully intergraular fracture surface observed in the 1-hour dwell loading region as shown in Figure 10. Different failure mechanisms under dwell fatigue crack loading have been discussed in depth elsewhere.[12] Note that the dwell crack growth rates measured for the as-received condition in the current study are similar to the FC condition published previously.[12] However, it seems that the

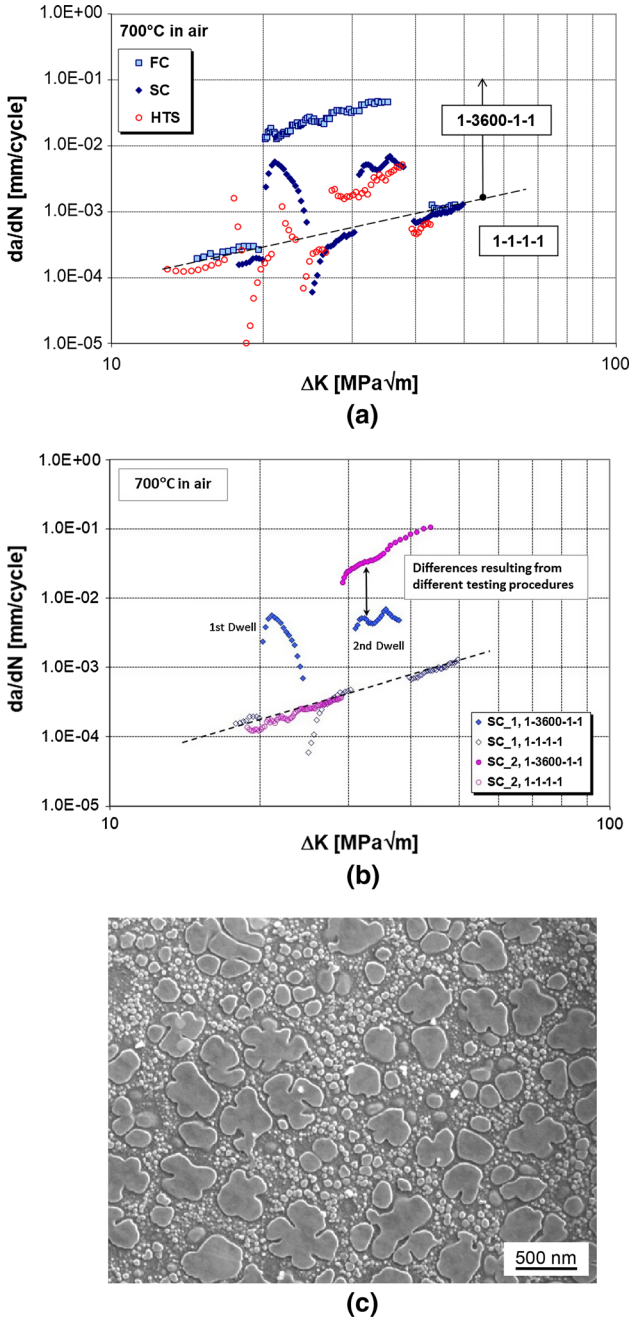

Fig. 8—Effects of starting microstructure (using data first published in Ref. [12]), (*a*), and initial ΔK, (*b*), on dwell fatigue crack growth resistance for a CG RR1000 at 700 °C in air. Note that the different microstructural conditions in (a) include fast cooled (FC) and slow cooled (SC) and high-temperature stabilize aging (HTS). The microstructure of SC (SC_1 in (b)) after testing is shown in (*c*).

previous batches of material display slightly better dwell crack growth resistance in overaged conditions, if we consider an on-test overaging time of 238 hours (at 700 °C) received in the case of SC_1 before reaching the second block of dwell loading and disregard any potential influence of stress on overaging. This is likely to result from microstructural variations between different batches, for example, grain size and its distribution, but further consideration is beyond the subject of the current study.

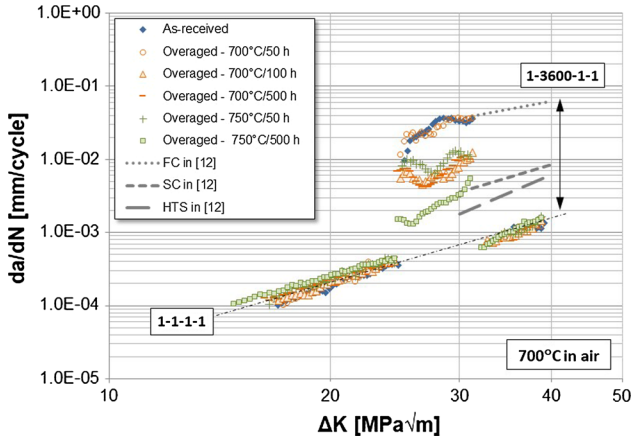

Fig. 9—The influence of isothermal treatment prior to testing on the dwell fatigue crack growth behavior of CG RR1000—the dashed lines are drawn through data first published in Ref. [12].

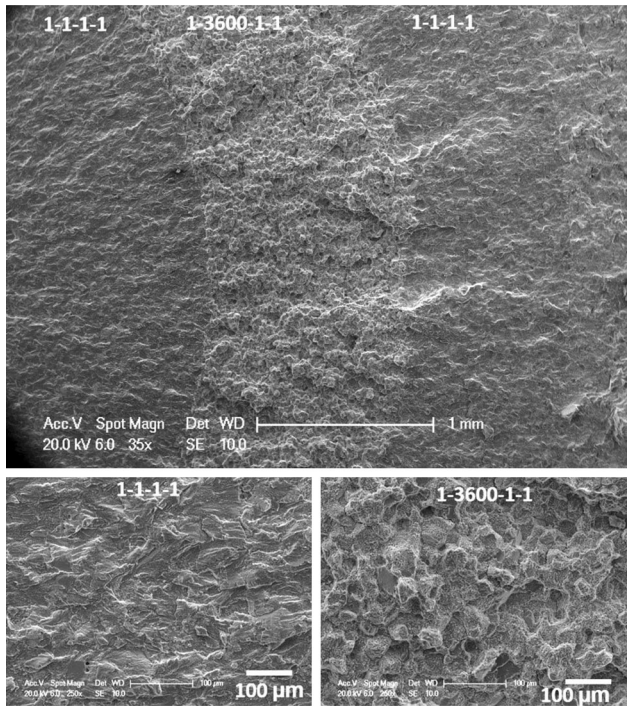

Fig. 10—Representative fractographs for different loading blocks applied during crack growth testing. Note that the ΔK values associated with the 1-1-1-1 and the 1-3600-1-1 regions are 22 and 28, respectively, and the crack growth direction is from left to right in all cases.

Figure 9 shows that overaging can improve dwell fatigue crack growth resistance. This is generally represented well with a plot of the crack growth rate at a stress intensity of $\Delta K < 30$ MPa√m for all specimens tested here against the mean tertiary γ' size as shown in Figure 11. Although there are deviations from a linear relationship (the most significant deviation from the linear relationship is for data from 100 hours of exposure at 700 °C, where measured crack growth rates are lower than predicted), a general trend of lower crack growth rates corresponding to coarser tertiary γ' sizes is

evident at a given ΔK. It is intriguing to see that an improvement in dwell crack growth resistance appears to be initiated after only 100 hours at 700 °C. For this particular condition, the changes of both tertiary and secondary γ' are so subtle that they cannot be identified by observation on SEM micrographs. However, TEM analysis does confirm coarsening of tertiary γ' has occurred after 100 hours thermal exposure at 700 °C, which is not observed after 50 hours, compare Figure 2(c) with Figures 2(a) and (b). Such coarsening behavior is also supported with further analysis from SEM micrographs as shown in Figure 3 which suggests that the coarsening of tertiary γ' obeys a power law if an initial period of ~ 50 hours is excluded. It is possible that an incubation period is needed before the onset of coarsening. It is hypothesized that resistance to dwell crack growth could improve soon after this incubation time while the average size of tertiary γ' still remains relatively small.

It is important to mention that dwell fatigue crack growth resistance is very sensitive to microstructure. As such, an ongoing challenge in all such studies is the possible variation in the starting microstructure of the "as-received" material (prior to heat treatment and/or subsequent mechanical testing). In the current study, attention has been made to keep the starting microstructure consistent. One obvious concern relates to the control of grain size, especially for the coarse-grained variants used here. In the current study, such variations have been minimized by test piece extraction from a localized position in the pancake forging. Even so it is possible that some results may have been affected by microstructural variables other than overaging. This makes precise interpretation of results from intermediate overaging conditions difficult. For example, similar crack growth behavior was seen after aging for 100 hours at 700 °C, 500 hours at 700 °C, and 50 hours at 750 °C.

As discussed by Li *et al.*,[12] acceleration of crack growth rates under sustained peak load in CG RR1000 at a temperature of 700 °C is largely environmentally assisted. A model of how oxides form and rupture, and subsequently affect dwell crack growth behavior is given elsewhere.[12] Environmentally assisted time-dependent crack growth is thought to depend heavily on the ability of the material to relieve stress around the crack tip. One approach to characterize this material property, albeit on round bar test pieces, is through stress relaxation testing. Such tests have been conducted here for the as-received and overaged (500 hours at 700 °C) samples. A comparison of their stress relaxation curves under a 1 pct constant strain is provided in Figure 12. At first glance, the two curves look similar (Figure 12(a)). A small difference in stress profiles is seen over the majority of the test period, but with the overaged sample consistently showing lower retained stress. By the end of the test duration of 50 hours, only a very small difference remains, ~40 MPa. However, a closer look at the stress relaxation behavior within the initial 1000 seconds (Figure 12(b)) reveals an important characteristic of the overaged sample which could be

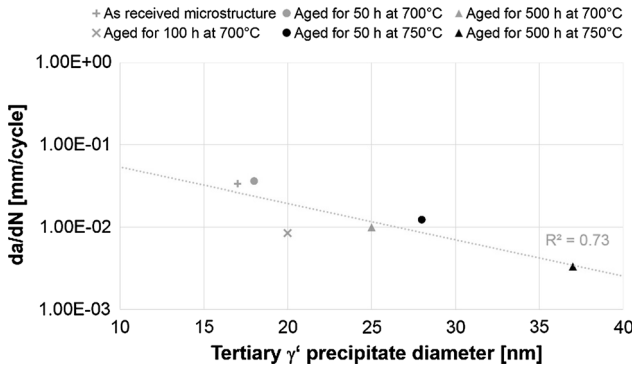

Fig. 11—Dwell fatigue crack growth rates of CG RR1000 at a stress intensity factor of $\Delta K = 30$ MPa$\sqrt{\text{m}}$ *vs* the respective tertiary γ' precipitate mean diameter.

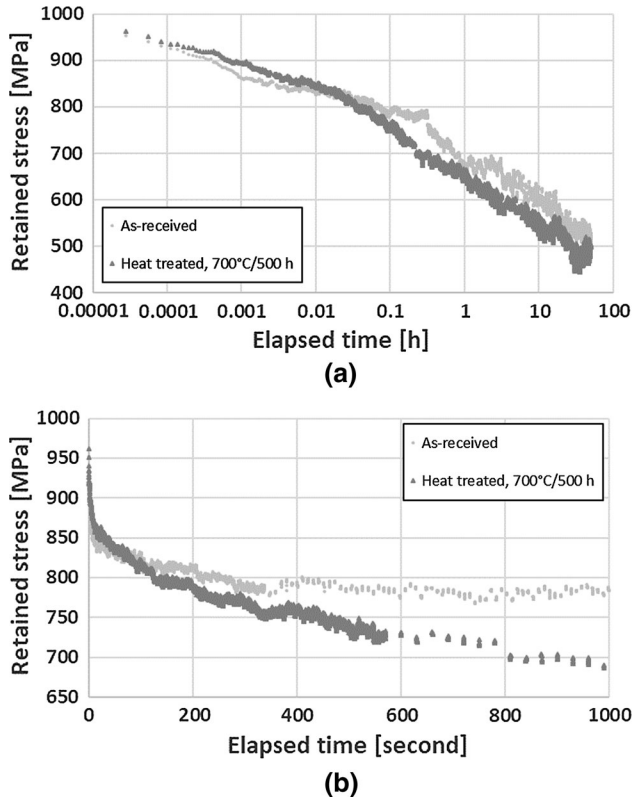

Fig. 12—Stress relaxation data of CG RR1000 tested at 700 °C in air with a constant strain of 1 pct for the as-received and overaged samples: (*a*) overview with logarithmic time scale and (*b*) first 1000 s in linear time scale.

important for promoting good dwell fatigue crack growth resistance. Immediately after application of 1 pct strain, the gradient of the stress relaxation for the overaged sample over 200 seconds is − 0.39 MPa/s. This is almost double that measured for the as-received sample, − 0.21 MPa/s. The stress relaxation rate is gradually reduced over time in both samples but a consistently higher rate is achieved for the overaged sample for up to 20 minutes. It is believed here that stress relaxation over a short period of time (<1 hours)

is most relevant to dwell fatigue crack growth behavior. This is similar to the concept of "remaining stress" proposed by Telesman *et al.*[23] observed for conditions where microstructural variations are greater. Here, the challenge is to apply this concept to microstructure with more subtle variations. Further characterization of stress relaxation behavior after different overaging conditions and associated deformation mechanisms are needed to support such arguments.

V. CONCLUSIONS

The impact of thermal exposure at 700 °C and 750 °C on dwell fatigue crack growth resistance has been studied in a coarse grain RR1000, together with a detailed characterization of secondary and tertiary γ' evolution using both SEM and STEM. The following conclusions can be drawn:

1. Coarsening of tertiary γ' has been studied in coarse grain RR1000 after thermal exposure (without being subject to stress) at both 700 °C and 750 °C. At 750 °C, coarsening is significantly faster than that at 700 °C, this is also accompanied by dissolution of tertiary γ' precipitates (only ~a third remain in terms of volume fraction after 500 hours exposure at 750 °C). No changes are observed in γ' size and distributions for up to 50 hours at 700 °C.
2. Coarsening of secondary and tertiary γ' follows Lifshitz–Slyozov–Wagner (LSW) theory at 700 °C up to 500 hours. In contrast, at 750 °C, secondary γ' undergoes a cyclic morphological evolution and neither secondary nor tertiary γ' obeys the classical diffusion-controlled coarsening relationship. This is suggested to result from an interaction between adjacent secondary γ' and tertiary γ' particles.
3. The coarsening of tertiary γ' precipitates is observed to increase the dwell crack growth resistance for tests carried out at 700 °C in air with a one-hour dwell time occurring at the maximum load. Increased dwell crack growth resistance is first observed in tests after (prior) overaging at 700 °C for 100 hours.
4. A general inverse relationship between crack growth rates at a ΔK of 30 MPa$\sqrt{\text{m}}$ and mean diameter of tertiary γ' is found for the dwell fatigue crack growth test conditions applied.
5. A limited study of stress relaxation behavior (in round bar test pieces) suggests that increased rates of relaxation are observed (especially for times of up to 20 minutes) after overaging for 500 hours at 700 °C.

ACKNOWLEDGMENTS

The current research was funded under the Engineering and Physical Sciences Research Council (EPSRC) - Rolls-Royce Strategic Partnership in Structural Metallic Systems for Gas Turbines. The provision of materials and supporting information from Rolls-Royce plc is gratefully acknowledged. The authors would like to acknowledge the assistance provided by Dr. Tim Doel in stress relaxation tests.

OPEN ACCESS

REFERENCES

1. R.C. Reed: *The Superalloys: Fundamentals and Applications*, 1st ed., Cambridge University Press, Cambridge, 2006, pp. 33–120.
2. R.J. Mitchell, J.A. Lemsky, R. Ramanathan, H.Y. Li, K.M. Perkins, and L.D. Connor: *Superalloys 2008—Proc. 11th Int. Symp. Superalloys*, Minerals, Metals & Materials Society, Warrendale, 2008, pp. 347–56.
3. A.J. Manning, D. Knowles, and C.J. Small: *A nickel base superalloy*, European Patent EP1 193 321 A1, 2002.
4. M.C. Hardy, B. Zirbel, G. Shen, and R. Shankar: *Superalloys 2004—Proc. 10th Int. Symp. Superalloys*, Minerals, Metals & Materials Society, Warrendale, 2004, pp. 83–90.
5. S. Everitt, M.J. Starink, and P.A.S. Reed: *Superalloys 2008—Proc. 11th Int. Symp. Superalloys*, Minerals, Metals & Materials Society, Warrendale, 2008, pp. 741–50.
6. M.A. Hicks and J.E. King: *Int. J. Fatigue*, 1983, vol. 5, pp. 67–74.
7. H. Ghonem, T. Nicholas, and A. Pineau: *Fatigue Fract. Eng. Mater. Struct.*, 1993, vol. 16, pp. 565–76.
8. S.A. Padula, A. Shyam, R.O. Ritchie, and W.W. Milligan: *Int. J. Fatigue*, 1999, vol. 21, pp. 725–31.
9. M.L. Brogdon and A.H. Rosenberger: *Superalloys 2008—Proc. 11th Int. Symp. Superalloys*, Minerals, Metals & Materials Society, Warrendale, 2008, pp. 583–88.
10. H. Yang, R. Bao, J. Zhang, L. Peng, and B. Fei: *Int. J. Fatigue*, 2011, vol. 33, pp. 632–41.
11. R. Jiang, S. Everitt, M. Lewandowski, N. Gao, and P.A.S. Reed: *Int. J. Fatigue*, 2014, vol. 62, pp. 217–27.
12. H.Y. Li, J.F. Sun, M.C. Hardy, H.E. Evans, S.J. Williams, T.J.A. Doel, and P. Bowen: *Acta Mater.*, 2015, vol. 90, pp. 355–69.
13. J.J. Schirra, P.L. R. Pratt, E. Hartford, E.S. Huron, K.R. Bain, D.P. Mourer, G. Electric, and A. Engines: *Superalloys 2004—Proc. 10th Int. Symp. Superalloys*, Minerals, Metals & Materials Society, Warrendale, Pennsylvania, 2004, pp. 341–50.
14. H.T. Pang and P.A.S. Reed: *Int. J. Fatigue*, 2008, vol. 30, pp. 2009–20.
15. J. Telesman, T. Gabb, A. Carg, P. Bonacuse, and J. Gayda: *Superalloys 2008—Proc. 11th Int. Symp. Superalloys*, Wiley, New York, 2008, pp. 807–16.
16. K. Maciejewski and H. Ghonem: *Superalloys 2012—Proc. 12th Int. Symp. Superalloys*, Wiley, New York, 2012, pp. 421–30.
17. M. Preuss, J.K.L. Pang, P.J. Withers, and G.J. Baxter: *Metall. Mater. Trans. A*, 2002, vol. 33, pp. 3215–25.
18. Y. Chen, R. Prasath Babu, T.J.A. Slater, M. Bai, R. Mitchell, O. Ciuca, M. Preuss, and S.J. Haigh: *Acta Mater.*, 2016, vol. 110, pp. 295–305.
19. I.M. Lifshitz and V.V. Slyozov: *J. Phys. Chem. Solids*, 1961, vol. 19, pp. 35–50.
20. C. Wagner: *Z. Elektrochem.*, 1961, vol. 65, pp. 581–91.
21. P.K. Rastogi and A.J. Ardell: *Acta Metall.*, 1971, vol. 19, pp. 321–30.
22. S. Zhao, X. Xie, G.D. Smith, and S.J. Patel: *Mater. Lett.*, 2004, vol. 58, pp. 1784–87.
23. J. Telesman, T.P. Gabb, and L.J. Ghosn: *Superalloys—Proc. 13th Int. Symp. Superalloys*, Wiley, Hoboken, 2016, pp. 551–60.